Neoclassical transport with non-trace impurities in density pedestals

S. Buller[1], I. Pusztai[1], M. Landreman[2]

[1] *Department of Physics, Chalmers University of Technology, Göteborg, Sweden*

[2] *Institute for Research in Electronics and Applied Physics, University of Maryland, USA*

The global confinement degradation when transitioning from carbon to metallic walls on various tokamaks, and the ability to recover confinement with impurity seeding, has been linked to the pedestal performance [1]. As turbulence is quenched in the pedestal, neoclassical effects are expected to play a role. We use the neoclassical solver PERFECT [2, 3] to study the collisional transport in pedestals in the presence of non-trace (i.e. $Z_{\text{eff}} - 1 = \mathcal{O}(1)$) nitrogen impurities. Our approach captures finite-orbit width effects in density pedestals with electrostatic ion confinement. We find that the radial coupling has a notable effect on fluxes several orbit widths away from the pedestal since they are carried mostly by super-thermal particles. Also, impurities tend to increase the neoclassical transport of toroidal angular momentum, which is non-negligible in the presence of orbit width scale profile variations.

Radially global δf drift-kinetics Steady-state neoclassical transport may be obtained from the time-independent full-f drift-kinetic equation $(\mathbf{b}v_\parallel + \mathbf{v}_D)\cdot\nabla f = C[f] + S$, with the gyrophase averaged distribution f, the drift velocity $\mathbf{v}_D$, the nonlinear collision operator C, and a source S needed for the steady state to be consistent with radial profile variations. The gradient is performed holding the total energy and the magnetic moment fixed. Species indices are suppressed. The full-f equation can be linearized when f varies on a scale L larger than the orbit width $\delta = \rho_p/L \ll 1$, where ρ_p is the poloidal gyroradius ($\sim$ orbit width). Assuming all low order moments and the electrostatic potential Φ obey $\delta \ll 1$ leads to the conventional local δf theory. However, linearization about a Maxwellian $f_M(\psi, W) = (m/2\pi T)^{3/2}\eta e^{-\frac{mW}{T}}$ is possible even if $\rho_p\{\frac{d\log\Phi_0}{dr}, \frac{d\log n}{dr}\} = \mathcal{O}(1)$, when $\rho_p\{\frac{d\log T}{dr}, \frac{d\log\eta}{dr}\} \ll 1$, which corresponds to electrostatic ion confinement and subsonic flows [3]. We introduced $\eta(\psi) = ne^{Ze\Phi_0/T}$, the flux surface average potential Φ_0, the density n and the temperature T, which are all flux functions, and we use the energy variable $W = v^2/2 + Ze\Phi_0/m$. The notation is standard or similar to that of [4]. Linearization yields the global δf equation

$$(\mathbf{b}v_\parallel + \mathbf{v}_D)\cdot\nabla g - C_l[g] - S = -\mathbf{v}_m\cdot\nabla f_M. \tag{1}$$

with $g = f - f_M(1 - Ze\Phi_1/T_0)$, the magnetic drift velocity $\mathbf{v}_m$, and $\Phi_1 = \Phi - \Phi_0$. Equation (1) differs from the local case by the source S and the term $\mathbf{v}_D\cdot\nabla g$ that gives radial coupling between nearby flux surfaces, and accounts for the strong radial electric field.

Simulation, inputs We performed PERFECT simulations using the model input profiles shown in Figure 1, which are constructed to have representative scale lengths of the n_e and T_e profiles reported in Fig. 16 of Ref. [5], while the Φ_0, n_z and $T_i = T_z$ profiles are chosen to satisfy our orderings. The profiles are plotted as functions of ψ^o, which is the poloidal flux ψ normalized and offset so that a typical trapped ion orbit has a width of $\Delta\psi^o = 1$, and $\psi^o = 0$ at the last closed flux surface. The local neoclassical solution is imposed as the boundary condition on both ends of the radial domain, and a buffer region with closed field lines and flattened profiles is employed for $\psi^o > 0$ (not shown), which would be the open field line region. The trace and non-trace impurity simulation inputs are obtained by scaling the impurity profile to achieve $Z_{\text{eff}} = 1.017$ and $Z_{\text{eff}} = 2.33$ in the core region, and keeping the n_i profile fixed.

The source S in (1) is taken to be a flux function and has two components of the form $\propto \left(\frac{v^2}{v_t^2} - \left\{\frac{5}{2}, \frac{3}{2}\right\}\right) e^{-v^2/v_t^2}$ that contribute to the {particle, energy} conservation equations ($v_t = \sqrt{2T/m}$ is the thermal speed). The radial variation of these sources is calculated by requiring the flux surface average density and pressure to be contained in f_M. The simulations use a Miller model geometry with parameters: $\kappa = 1.58$, $s_\kappa = 0.479$, $\delta = 0.24$, $s_\delta = 0.845$, $dR_0/dr = -0.14$, $q = 3.5$, $\epsilon = 0.263$.

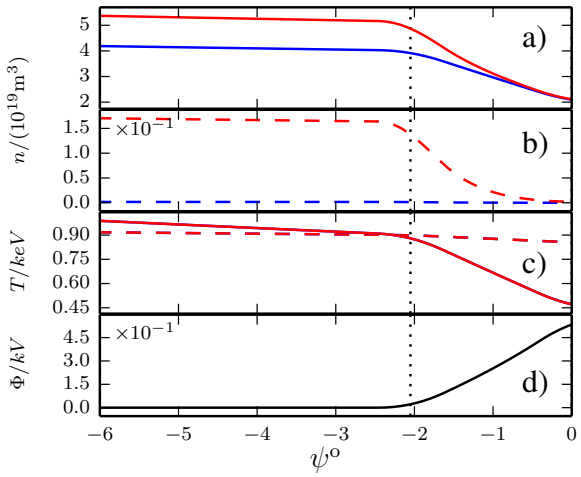

Figure 1: Input profiles. a) n_e; b) n_z; c) T_e (solid) and $T_i = T_z$ (dashed); d) Φ_0. Blue (red) lines in (a,b) correspond to the trace (non-trace) case.

Neoclassical fluxes for trace and non-trace impurities The radial particle fluxes Γ and the total conductive heat flux q are shown in Figure 2, with blue (red) lines corresponding to results from trace (non-trace) simulations. Global (local) simulation results are plotted with solid (dashed) lines. We generally observe that it takes several orbit widths for the neoclassical quantities to approach their local values away from the pedestal. Without showing a corresponding figure, we note that the flows and poloidal density perturbations exhibit similar behavior [4]. In the core, when impurities are non-trace, they tend to have a particle flux opposing that of the ions, and the electron fluxes are small in $\sqrt{m_e/m_i}$. In the pedestal, the neoclassical electron particle transport (Figure 2b) is not negligible compared to the ion transport, due to the large flow of electrons compared to the ion species. Intrinsic ambipolarity is a property of the *local* drift kinetic equation, however in the vicinity of the pedestal the neoclassical particle transport is not intrinsically ambipolar. These two effects allow the impurities and main ions to diffuse in

the same direction radially, even for non-trace impurity concentrations (for instance at $\psi^o = -3$, compare solid red curves in Figure 2a and c). The small electron orbit width keeps the electron transport close to its local value, while the ions display significant differences between local and global results.

The total conductive heat flux shown in Figure 2d is dominated by the contribution of the main ions and is significantly reduced inside the pedestal compared to its local value. Such a reduction is predicted by analytical theories [6, 7, 8] retaining the $\mathbf{v}_{E\times B}\cdot\nabla g$ term (where $\mathbf{v}_{E\times B}$ is the $E\times B$ drift velocity from Φ_0), due to the shift of the trapped region toward the tail of the distribution. However in the simulations the radial coupling – that is the $\mathbf{v}_m\cdot\nabla g$ term – is seen to play a more prominent role in the reduction, by smoothing the heat flux (q) profile. The reduction in the total conductive heat flux is stronger in the non-trace case, as the quantity $U = |\mathbf{v}_{E\times B}|B/(v_t B_p)$ – quantifying the relevance of $\mathbf{v}_{E\times B}$ in the poloidal particle motion – is larger for the impurities than for bulk ions.

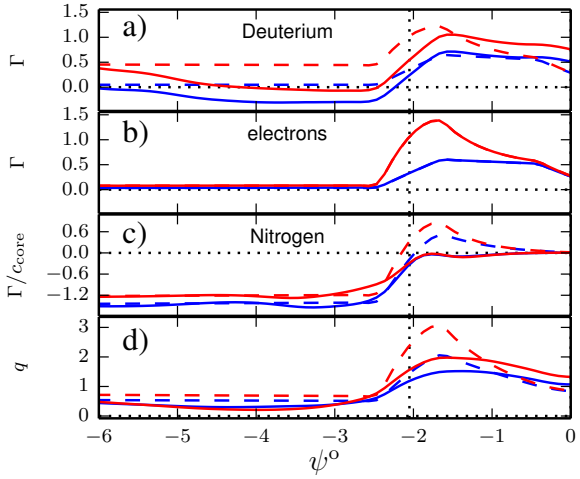

Figure 2: Radial particle flux $[10^{19}\mathrm{s}^{-1}\mathrm{m}^{-2}]$ of bulk ions (a), electrons (b), impurities (c, normalized with the core impurity concentration n_z/n_i). Total convective heat flux $[10^{19}\mathrm{keVs}^{-1}\mathrm{m}^{-2}]$) (d). Blue (red) lines correspond to the trace (non-trace) case.

In local neoclassical theory both the radial current j_r and the radial flux of the toroidal angular momentum Π are formally small and they cannot be evaluated without going to higher order in δ, while they are finite in the presence of orbit width scale radial variations. In our simulations the torque on the plasma due to j_r is balanced by a finite divergence of Π. The normalized momentum flux $\hat{\Pi}^* = \Pi\left(d_\psi T_\mathrm{D}\right)/\left(q_\mathrm{D} R m_\mathrm{D} V_\mathrm{torD} d_\psi n_\mathrm{D}\right)$ – a proxy for the neoclassical effective Prandtl number – is shown in Figure 3. Here V_tor is the toroidal rotation speed, the D subscript refers to deuterium, and all quantities except Π and R are evaluated at $\psi^o = -1.2$. Notably $\hat{\Pi}^*$ has a magnitude $0.1 - 0.3$ in the pedestal, which is comparable to the turbulent Prandtl number reported for core

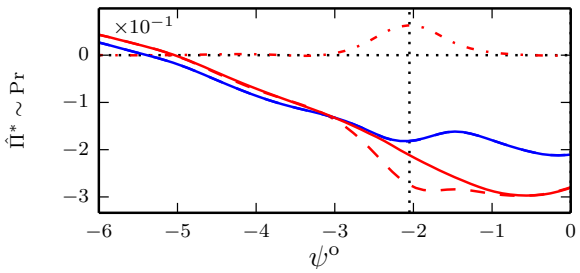

Figure 3: Angular momentum transport normalized to be a proxy for the neoclassical Prandtl number. Blue line: trace impurity case. Red lines: non trace impurities, where deuterium (dashed), nitrogen (dash-dotted), and their sum (solid) are shown.

plasmas (e.g. KSTAR[9], JET[10]). Thus neoclassical transport may carry a significant portion of the momentum flux in the vicinity of the pedestal, noting that the ion heat flux is experimentally observed to be at neoclassical level, assuming that our result extrapolates to sharp ion temperature pedestals. By comparing trace and non-trace lines in Figure 3, we thus see that impurities have a significant effect on the pedestal momentum transport.

Conclusions We have modeled neoclassical particle, heat and momentum fluxes in density pedestals in the presence of non-trace impurities, accounting for effects from the strong electric field and radial coupling due to finite orbit width. We see that global effects are important both inside and several thermal orbit widths away from the pedestal. The violation of intrinsic ambipolarity, and the non-negligible electron particle transport, can lead to an impurity particle flux in the same direction as the bulk ions even when the impurities are non-trace. In the pedestal the neoclassical conductive heat flux is smaller than local codes would predict, and this reduction is stronger with non-trace impurities. In the presence of orbit width scale profile variations the neoclassical radial transport of toroidal angular momentum is not negligibly small (effective Prandtl number $\sim 10\%$), and it is significantly increased in magnitude by impurities.

We considered neoclassical processes in isolation, where non-neoclassical processes appear as sources to cancel the divergence of the neoclassical fluxes. In steady state the predicted non-ambipolar fluxes and finite momentum transport should be canceled by non-neoclassical phenomena not modeled here, such as turbulence. This may be related to the improved pedestal performance with increased impurity seeding, as sharper profile variations would typically result in increased turbulent intrinsic momentum transport, encouraging the development of sheared pedestal flows.

Acknowledgments We are grateful for fruitful discussions with S. Newton and J. Omotani. SB and IP were supported by the INCA grant of Vetenskapsrådet (Dnr. 330-2014-6313), and ML was supported by the USDoE grants DEFG0293ER54197 and DEFC0208ER54964. The simulations used computational resources of Hebbe at C3SE (C3SE2016-1-10 & SNIC2016-1-161).

References

[1] M.N.A Beurskens et al., Plasma Phys. Control. Fusion **55**, 124043 (2013)
[2] M. Landreman et al., Plasma Phys. Control. Fusion **56**, 045005 (2012)
[3] M. Landreman and D.R. Ernst, Plasma Phys. Control. Fusion **54**, 115006 (2012)
[4] I Pusztai et al., Plasma Phys. Control. Fusion **58**, 085001 (2016)
[5] C.F. Maggi et al., Nuclear Fusion **55**, 113031 (2015)
[6] G. Kagan and P.J. Catto, Plasma Phys. Control. Fusion **52**, 055004 (2010)
[7] I. Pusztai and P.J. Catto, Plasma Phys. Control. Fusion **52**, 075016 (2010)
[8] P.J. Catto et al., Plasma Phys. Control. Fusion **55**, 045009 (2013)
[9] S.H. Ko et al., Phys. Plasma **23** 062502 (2016)
[10] T. Tala et al., Phys. Rev. Lett. **102** 075001 (2009)